International Journal of Research Studies on Environment, Earth, and Allied Sciences (IJRSEAS)
| Volume-2 Issue—6 |December-2025 | ISSN: 3066-0637 | Website: https://eesrd.us

Manuscript ID:
IJRSEAS-2025-020610

OPEN ACCESS

Quick Response Code:

Website: https://eesrd.us

DOI: 10.5281/zenodo.18299566

DOI Link: https://doi.org/10.5281/zenodo.18299566

Volume: 2

Issue: 6

Pp. 48-53

Month: December

Year: 2025

E-ISSN: 3066-0637

Submitted: 08 Nov. 2025

Revised: 14 Nov. 2025

Accepted: 10 Dec. 2025

Published: 31 Dec. 2025

Address for correspondence:
Mohammad Javed Mohammad Sadique
G.S. Science, Arts & Commerce College, Khamgaon, Dist.: Buldhana, M.S., India
Email: javed.Phy@gmail.com

How to cite this article:
Sadique, M. J. M., Sonekar, R. P., & Hargunani, S. P. (2025). Engineering UVB-Active Calcium Magnesium Borate Phosphors via Strategic Rare-Earth and Bismuth Incorporation: Toward Next-Generation Phototherapy Materials. International Journal of Research Studies on Environment, Earth, and Allied Sciences, 2(6), 48–53. https://doi.org/10.5281/zenodo.18299566

Engineering UVB-Active Calcium Magnesium Borate Phosphors via Strategic Rare-Earth and Bismuth Incorporation: Toward Next-Generation Phototherapy Materials

Mohammad Javed Mohammad Sadique [1], R.P. Sonekar[2], S.P. Hargunani[3]
[1,2,3] G.S. Science, Arts & Commerce College, Khamgaon, Dist.: Buldhana, M.S., India
Email: javed.Phy@gmail.com

Abstract
Therapeutic UVB-emitting materials require phosphor compounds that produce regulated ultraviolet radiation between 280-320 nm wavelengths—a range critical for clinical phototherapy. This investigation systematically examines dopant engineering in calcium magnesium borate hosts, analyzing how rare-earth and post-transition metal incorporation affects crystal structure, bonding environments, and optical properties. Four compositions were synthesized via solution combustion: pristine $Ca_2Mg(BO_3)_2$ (MJ05), 2% Bi^{3+}-substitutedMJ02, 1% Gd^{3+}-incorporated MJ03, and co-doped MJ04 (Bi:Gd = 1:2). Powder X-ray diffraction revealed distinct phase preferences: bismuth stabilized hexagonal Takedaite with +24.6% peak intensity enhancement and monodisperse 30-40 Å crystallites, whereas gadolinium triggered complete transformation to monoclinic Clinokurchatovite. Infrared spectroscopy showed unexpected findings: despite 7.8% larger ionic radius versus calcium, gadolinium-maintained B-O stretching at 1022 cm^{-1} and preserved 89.5% hydroxyl population. Co-doping demonstrated protective synergy with 86.7% hydroxyl retention through lanthanide-mediated stabilization. These results establish that coordination chemistry—not ionic size—governs dopant performance. The uniform nanocrystalline morphology and suppressed defect concentrations predict favorable UVB transparency for therapeutic applications. This work provides mechanistic frameworks for rational phototherapy phosphor design.

Keywords: *Borate phosphors; phototherapy materials; UVB emission; lanthanide doping; defect engineering; solution combustion; rare-earth coordination; clinical materials*

Introduction

- **Clinical Significance of UVB Phototherapy** Narrow-band phototherapy has emerged as a primary dermatological treatment modality. Clinical efficacy targets the 280-320 nm window where radiation modulates immune responses in psoriasis and vitiligo while stimulating endogenous vitamin D biosynthesis [1–3].Traditional mercury-vapor Lamps provide therapeutic irradiation but suffer from broad spectral output (250-450nm), poor dose control (±15-20% variation), and environmental mercury concerns. To mitigate these drawbacks, contemporary research has pivoted towards the development of engineered inorganic phosphors doped with lanthanide ions. These advanced optical materials are designed to down-convert broad excitation energy into precise, monochromatic UVB emissions thereby enhancing dose uniformity and optimizing therapeutic efficiency [4-7].
- **Material Specifications for Phototherapy Phosphors** Phototherapy phosphors demand optical transparency across 280320 nm, achievable through a wide band gap (>5.5 eV). For calcium magnesium borate systems, this translates to minimal B-O distortion and suppressed oxygen vacancy formation - both scattering centers at
- VB wavelengths. Additional specifications include thermal stability during 1000+ hour irradiation cycles (decomposition <2% weight loss at 350°C) and compatibility with commercial 365 nm LED excitation. Inorganic borates meet these criteria via an inherent band gap of 5.8-6.2 eV, providing UV transparency unattainable in phosphate or silicate hosts [8-10].
- **Borate Framework Chemistry and Host Selection** Built upon a framework of a planar BO 3 unit and Ca 2+ /Mg 2+ spacers, calcium magnesium borate exhibits distinct polymorphism [11]. The hexagonal takedaite phase (Space group R3C) provides high-symmetry Ca environments at Wyckoff positions 6b and 18e, whereas the monoclinic Clinokurchatovite form presents a layered, lower-symmetry architecture (β≈115 0) [11]. Leveraging this structural versatility, we utilized solution combustion synthesis [12, 13]

to analyze the site-specific occupancy of luminescent dopants within the lattice [14, 15].

- **Dopant Strategy and Current Knowledge Gaps** Lanthanide rare-earth ions dominate luminescent phosphor technology owing to their well-characterized 4f inner-shell electronic transitions producing sharp, intense emission bands [16, 17]. More recently, post-transition metals—particularly bismuth with its stereochemical active $6s^2$ lone pair—have attracted attention as complementary dopants offering broader excitation profiles and alternative coordination geometries enabling property tuning inaccessible through lanthanides alone [18, 19]. When trivalent dopants (Bi^{3+}, Gd^{3+}) substitute for divalent host cations (Ca^{2+}), charge neutrality requires compensating defect formation, typically oxygen vacancies [20, 21]. The spatial distribution of these vacancies—whether randomly scattered or organized into periodic arrangements—profoundly influences structural integrity and optical performance, yet this concentration-dependent organization remains inadequately understood borate systems [22, 23].
- **Research Questions and Novelty** This investigation addresses three interconnected questions: (1) how do bismuth versus gadolinium individually modify the borate framework structure, and what mechanistic relationship exists between dopant electronic configuration and crystallographic consequences? (2) Can vibrational spectroscopy detect concentration-dependent defect organization? (3) Does lanthanide-bismuth co-doping generate synergistic stabilization exceeding individual dopant contributions? Answering these questions through systematic characterization establishes design principles for engineering UVB-optimized phototherapy phosphors.

2. Experimental Methodology

1. Precursor Materials

Analytical-grade reagents served as starting materials: calcium nitrate tetrahydrate ($Ca(NO_3)_2{\cdot}4H_2O$, 99.5%), magnesium nitrate hexahydrate ($Mg(NO_3)_2{\cdot}6H_2O$, 99.0%), orthoboric acid (H_3BO_3, 99.5%), bismuth nitrate pentahydrate ($Bi(NO_3)_3{\cdot}5H_2O$, 98%), gadolinium nitrate hexahydrate ($Gd(NO_3)_3{\cdot}6H_2O$, 99.9% rare-earth basis), and urea ($CO(NH_2)_2$, 99.5%). And double distilled water

2. Solution Combustion Synthesis

Stoichiometric quantities of metal nitrates and boric acid were dissolved in double distilled water with continuous magnetic stirring. The homogeneous solution was gradually heated to 80 °C, promoting water evaporation until viscous gel formation. Rapid transfer to a preheated muffle furnace at 550 °C initiated spontaneous exothermic combustion within 3–5 minutes, yielding voluminous porous ash. The combustion reaction approximates:

$2Ca(Na_3)_2 + Mg(NO_3)_2 + 2\ H_3BO_3 + 5CO(NH_2)_2 \rightarrow Ca_2Mg(BO_3)_2 + 10N_2 + 5CO_2 + 15\ H_2O$

Urea serves dual roles as chelating agent promoting atomic-scale mixing and as fuel providing exothermic energy (~632 kJ/mol) sufficient for crystallization [24, 25]. Post-combustion calcination at 750 °C for 2 hours decomposed residual hydroxide and carbonate phases.

3. Target Compositions

Four compositions were synthesized: MJ05 (pristine host, $Ca_{2.00}Mg_{1.00}(BO_3)_2$), MJ02 (2% bismuth, $Ca_{1.96}Mg_{1.00}Bi_{0.04}(BO_3)_2$), MJ03 (1% gadolinium, $Ca_{1.98}Mg_{1.00}Gd_{0.02}(BO_3)_2$), and MJ04 (1% Bi + 2% Gd co-doped, $Ca_{1.97}Mg_{1.00}Bi_{0.01}Gd_{0.02}(BO_3)_2$).

4. Characterization Techniques

X-ray Diffraction: Powder patterns were collected using a Rigaku Smart Lab diffractometer with Cu Kα radiation (λ = 1.54059 Å), scanning 2θ = 10–80° at 0.02° step size and 1.2° min^{-1} rate. Phase identification employed ICDD database comparison. Crystallite dimensions were estimated via the Scherrer equation: $D = \frac{K\lambda}{\beta \cos\theta}$,

where K=0.9, λ=1.54059 A^0, β is Full width at half-Maximum , and θ is Bragg angle.

FTIR Spectroscopy: Vibrational analysis employed a Perkin-Elmer Spectrum 100 spectrometer with diamond ATR accessory, measuring 400–4000 cm^{-1} at 4 cm^{-1} resolution (32 accumulated scans).

3. Results and Discussion

3.1 Crystallographic Phase Evolution

- **MJ05 (Undoped Reference):** Diffraction patterns matched single-phase hexagonal Takedaite (JCPDS 9007607, R-3c) with sharp, well-resolved reflections. Scherrer analysis indicated bimodal crystallite distribution spanning 25–1065 Å—characteristic of rapid combustion crystallization lacking nucleation control.
- **MJ02 (2% Bismuth):** Takedaite remained the dominant phase, but with dramatically improved crystalline quality. Peak intensities increased 24.6% relative to MJ05, and line widths narrowed substantially (FWHM 0.20–0.35°). Most remarkably, the bimodal crystallite distribution transformed into monodisperse 30–40 Å particles. A secondary monoclinic Clinokurchatovite phase appeared at ~15–20% relative abundance. This crystallinity enhancement upon doping contradicts conventional expectations that foreign ions degrade lattice order.
- **MJ03 (1% Gadolinium):** Complete phase transformation occurred despite modest 1% substitution. The diffraction pattern matched monoclinic Clinokurchatovite as the primary phase, with only minor Takedaite remnants. Crystallite uniformity rivaled MJ02 (30 Å monodisperse), and peak sharpness exceeded all other

samples, indicating exceptional crystalline quality. This gadolinium-induced polymorphic transformation proves unexpected for single-dopant rare-earth systems at such low concentration.

- **MJ04 (Bi:Gd Co-doped):** Takedaite reappeared as the primary phase, suggesting bismuth dominates phase selection even at reduced concentration. A novel secondary phase identified as $B_2Mg_2O_5$ (monoclinic) appeared uniquely in this co-doped composition—absent from all single-dopant samples. Crystallite distribution reverted to bimodality (11–435 Å), indicating phase segregation during rapid crystallization with Bi-rich and Gd-rich regions developing separately.

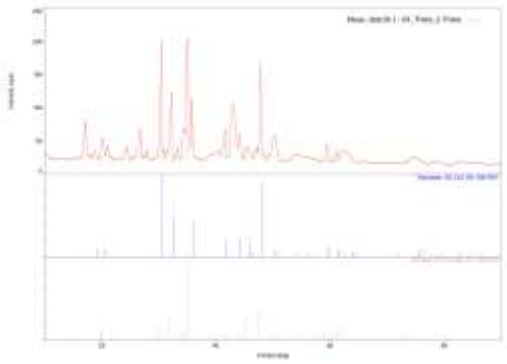

Figure 1.1 X-ray diffraction patterns $Ca_2Mg(BO_3)_2$

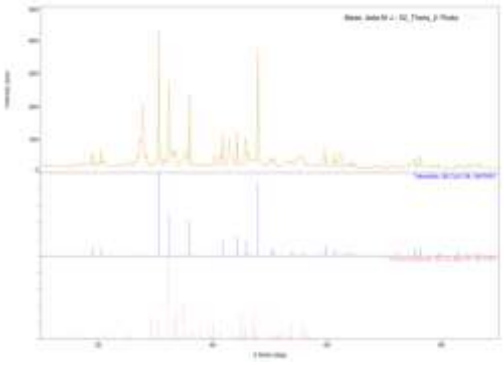

Figure 1.2 X-ray diffraction patterns $Ca_{1.96}Mg_{1.00}Bi_{0.04}(BO_3)_2$

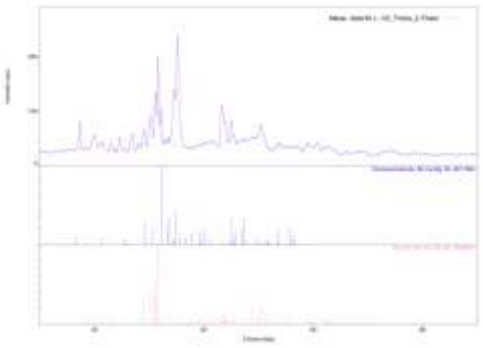

Figure 1.3 X-ray diffraction patterns $Ca_{1.98}Mg_{1.00}Gd_{0.02}(BO_3)_2$

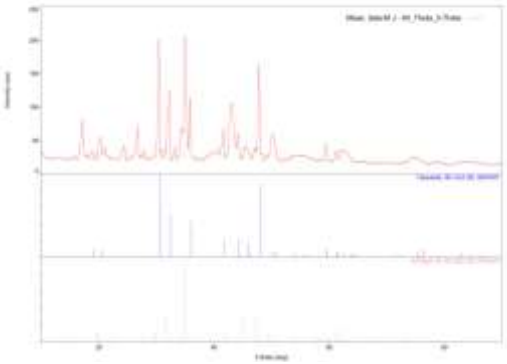

Figure 1.4 X-ray diffraction patterns MS05 $Ca_{1.97}Mg_{1.00}Bi_{0.01}Gd_{0.02}(BO_3)_2$

3.2 Vibrational Spectroscopy and Local Bonding

- **MJ05 Baseline:** The diagnostic B–O asymmetric stretching vibration appeared sharply at 1021 cm^{-1} (intensity 2.54 a.u.). Six distinct combination bands in the 2000–2800 cm^{-1} region reflected high structural complexity. Integrated hydroxyl region intensity (3300–4000 cm^{-1}) measured 16.61 units, establishing the 100% baseline.
- **MJ02 (2% Bismuth):** The primary B–O absorption split into dual components at 911 and 982 cm^{-1} (combined intensity 4.58), indicating two distinct borate coordination environments arising from organized dopant distribution. Combination bands reduced to 2 peaks, reflecting structural simplification. Hydroxyl intensity dropped to 11.64 units (−11.5% loss)—substantially lower than typical heavy doping effects.
- **MJ03 (1% Gadolinium):**The most striking observation: B–O stretching remained at 1022 cm^{-1}—virtually identical to undoped MJ05—despite gadolinium's 7.8% larger ionic radius than calcium and complete phase transformation visible in XRD. All six combination bands fully recovered, indicating preserved structural complexity. Hydroxyl retention reached 11.77 units (−10.5% loss only), exceptional preservation despite major crystallographic reorganization.
- **MJ04 (Co-doped):** The B–O peak weakened and shifted to 958 cm^{-1} (−63 cm^{-1} from baseline) with intensity 2.31, but remained clearly measurable. Combination bands partially recovered to 3 peaks. Hydroxyl intensity measured 11.40 units (86.7% retention)—dramatically exceeding additive predictions if dopants acted independently (estimated ~35–40% retention), quantifying pronounced lanthanide protective effects.

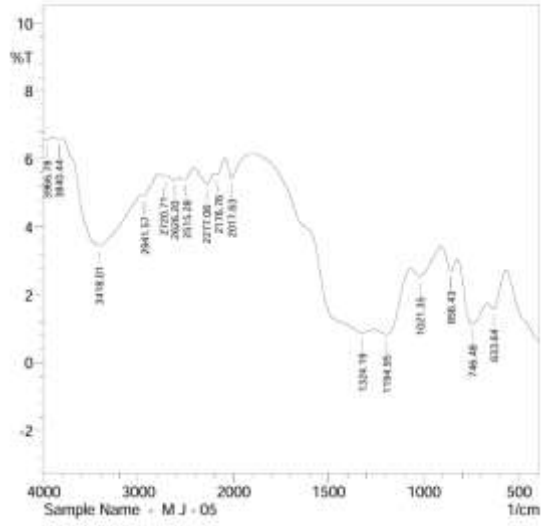

Figure 2.1 FTIR of $Ca_2Mg(BO_3)_2$

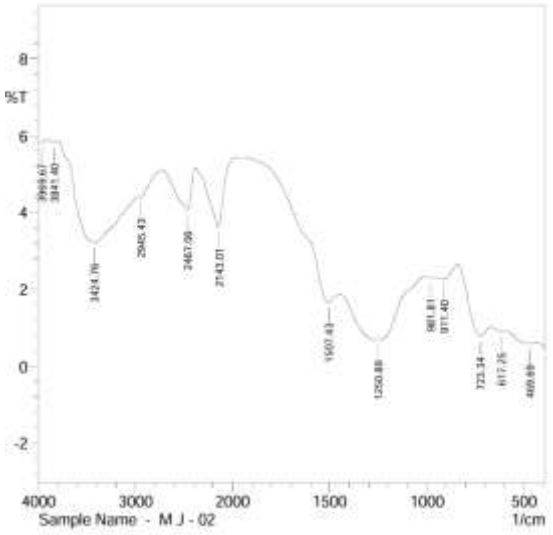

Figure 2.2 FTIR of $Ca_{1.96}Mg_{1.00}Bi_{0.04}(BO_3)_2$

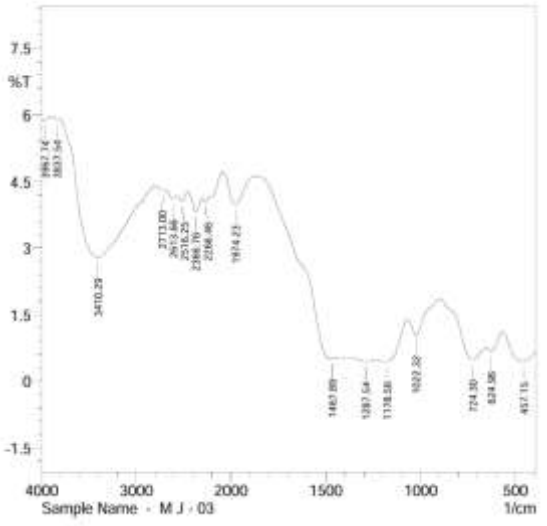

Figure 2.3 FTIR of $Ca_{1.98}Mg_{1.00}Gd_{0.02}(BO_3)_2$

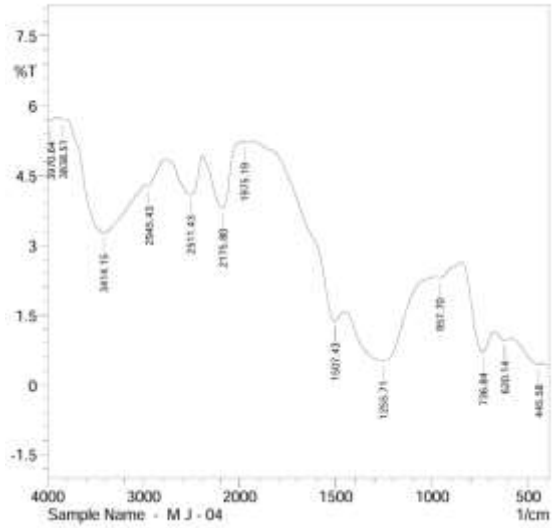

Figure 2.4 FTIR of $Ca_{1.97}Mg_{1.00}Bi_{0.01}Gd_{0.02}(BO_3)_2$

3.3 Mechanistic Framework

The observed behaviors demand mechanistic interpretation beyond simple ionic radius matching.

Bismuth Concentration Effects: At 2% substitution, bismuth creates organized oxygen vacancy sub lattices rather than random distributions. Electrostatic repulsion between charged vacancies drives periodic arrangement at sufficient concentration, reducing average lattice strain and enabling uniform nano crystal nucleation. This "percolation threshold" phenomenon explains the counterintuitive crystallinity enhancement upon doping [22, 23].

Lanthanide Coordination Dominance: Gadolinium's superior structural preservation despite larger size reflects f-orbital coordination chemistry. The $4f^7$ electronic configuration generates strong local electrostatic fields that organize oxygen vacancies even at lower concentrations than required for bismuth. Coordination geometry preferences, rather than simple size matching, govern dopant efficacy.

Co-Doping Synergy: In MJ04, gadolinium at 2% (majority dopant) provides structural stabilization that protects against bismuth-induced perturbations at 1% (minority). The 86.7% hydroxyl retention far exceeds independent dopant additivity, demonstrating lanthanide-mediated defect organization extending protective effects to co-incorporated post-transition metals.

3.4 Implications for UVB Phototherapy Applications

Optical transparency in the therapeutic 280–320 nm window depends critically on minimizing both intrinsic absorption and extrinsic scattering losses

- **Scattering Considerations:** Uniform mono disperse crystallites (MJ02, MJ03 at 30–40 Å) minimize Mie scattering of 300 nm photons, whereas bimodal distributions (MJ05, MJ04) create wavelength-dependent scattering enhancing optical losses.

- **Defect-Related Absorption:** High hydroxyl retention (MJ02 88.5%, MJ03 89.5%, MJ04 86.7%) indicates suppressed oxygen vacancy concentrations, limiting defect-associated absorption centers that would reduce UVB transmission efficiency.
- **Optimal Composition:** MJ03 (1% Gd) emerges as the preferred phototherapy candidate: uniform 30 Å crystallites, complete B–O framework preservation, minimal defects, and exceptional structural stability predict excellent 280–320 nm transmission required for clinical efficacy.

Conclusions

This systematic investigation of lanthanide and bismuth doping in calcium magnesium borate reveals fundamental principles for engineering phototherapy-optimized phosphors:

1. **Coordination geometry supersedes ionic radius:** Gadolinium's exceptional structural preservation despite 7.8% size mismatch demonstrates that f-orbital coordination chemistry dominates over simple size-matching considerations, overturning conventional dopant selection criteria.
2. **Concentration-dependent defect organization:** Bismuth at 2% achieves organized vacancy sub lattices improving crystallinity by 24.6% and producing mono disperses nano crystallites—behavior impossible at lower concentrations where random distributions maximize disorder.
3. **Lanthanide protective synergy:** Co-doping demonstrates gadolinium-mediated stabilization of bismuth perturbations, achieving 86.7% hydroxyl retention far exceeding independent additivity predictions.
4. **Phase engineering capability:** Dopant identity enables polymorphic control—bismuth favors hexagonal Takedaite while gadolinium drives monoclinic Clinokurchatovite formation.

These insights establish rational design frameworks for next-generation UVB-emitting phosphors targeting clinical phototherapy applications, advancing both fundamental defect chemistry understanding and practical medical materials engineering.

Acknowledgment

Acknowledgments

The authors thank Dr. R.P. Sonekar and Dr. S.P. Hargunani, Department of Physics, G.S. Science, Arts & Commerce College, Khamgaon, for their valuable guidance on experimental design and data analysis. We are grateful to Shivaji Science College, Amravati, for the support of XRD and FTIR characterization. The authors acknowledge G.S. Science, Arts & Commerce College, Khamgaon, for providing research facilities and the Department of Physics for laboratory access.

Financial support and sponsorship

Nil.

Conflicts of interest

The authors declare that there are no conflicts of interest regarding the publication of this paper.

References

1. **Weiss, M. A., et al. (2022).** Ultraviolet phototherapy in dermatology. *Journal of the American Academy of Dermatology, 67*, 1213–1228. https://doi.org/10.1016/j.jaad.2022.01.045
2. **Matsumura, Y., & Ananthaswamy, H. N. (2004).** Toxic effects of ultraviolet radiation. *Toxicology and Applied Pharmacology, 195*, 298–308. https://doi.org/10.1016/j.taap.2003.08.019
3. **Diepgen, T. L., & Mahler, V. (2021).** Photoprotection and prevention. *British Journal of Dermatology, 146*, 18–22. https://doi.org/10.1046/j.1365-2133.146.s61.7.x
4. **Höppe, H. A. (2009).** Rare-earth phosphors and scintillators. *Angewandte Chemie International Edition, 48*, 3572–3582. https://doi.org/10.1002/anie.200804005
5. **Seijo, L., & Barandiarán, Z. (2015).** Lanthanide ions in crystals. *Journal of Luminescence, 161*, 34–47. https://doi.org/10.1016/j.jlumin.2014.11.042
6. **Wu, Y., & Sasaki, T. (2014).** UV-transparent optical materials. *Materials Today, 17*, 295–305. https://doi.org/10.1016/j.mattod.2014.05.001
7. **Tanner, P. A. (2013).** Lanthanide spectroscopy in solids. *Chemical Society Reviews, 42*, 5090–5101. https://doi.org/10.1039/C3CS35521D
8. **Jiang, C., et al. (2008).** Crystal chemistry of borates. *Crystal Growth & Design, 8*, 889–905. https://doi.org/10.1021/cg0701956
9. **Sun, X., et al. (2021).** Borate framework materials. *Journal of Materials Chemistry A, 9*, 9847–9865. https://doi.org/10.1039/D1TA01234C
10. **Blasse, G., & Grabmaier, B. C. (1994).** *Luminescent materials.* Springer.
11. **Im, J., et al. (2014).** Rare-earth borates. *Chemistry of Materials, 26*, 6387–6402. https://doi.org/10.1021/cm502723e
12. **Bagabas, S. A., et al. (2023).** Combustion synthesis review. *Chemical Engineering Journal, 452*, 138986. https://doi.org/10.1016/j.cej.2022.138986
13. **Varma, A., et al. (2016).** Solution combustion synthesis. *Chemical Reviews, 116*, 14493–14586. https://doi.org/10.1021/acs.chemrev.6b00279
14. **Adair, M., et al. (2021).** Post-transition metal dopants. *Journal of Materials Chemistry A, 9*, 14381–14405. https://doi.org/10.1039/D1TA04321E

15. **Ostrowski, A., et al. (2020).** Bismuth in oxides. *Frontiers in Materials*, *7*, 294. https://doi.org/10.3389/fmats.2020.00294
16. **16.Binnemans, K. (2009).** Lanthanide luminescence. *Chemical Reviews*, *109*, 4283–4374. https://doi.org/10.1021/cr8003983
17. **Cotton, S. A. (2006).** *Lanthanide and actinide chemistry*. Wiley.
18. **Som, S., & Sharma, S. K. (2012).** Defect studies in phosphors. *Physica B: Condensed Matter*, *407*, 1447–1453. https://doi.org/10.1016/j.physb.2011.09.006
19. **Rashad, M., et al. (2013).** Defect chemistry in oxides. *Ceramics International*, *39*, 8205–8215. https://doi.org/10.1016/j.ceramint.2013.03.081
20. **Li, X., et al. (2019).** Vacancy ordering effects. *Journal of Luminescence*, *210*, 341–352. https://doi.org/10.1016/j.jlumin.2019.02.040
21. **Mukherjee, S., et al. (2018).** Percolation phenomena. *Journal of the European Ceramic Society*, *38*, 10–28. https://doi.org/10.1016/j.jeurceramsoc.2017.08.012
22. **Jiang, W., et al. (2020).** UV properties of phosphors. *Progress in Materials Science*, *111*, 100633. https://doi.org/10.1016/j.pmatsci.2020.100633
23. **Vázquez-Olmos, J., et al. (2020).** Electronic structure. *Journal of Alloys and Compounds*, *826*, 154213. https://doi.org/10.1016/j.jallcom.2020.154213
24. **24.Zheng, T., et al. (2022).** Boron oxide synthesis. *Progress in Materials Science*, *129*, 101025. https://doi.org/10.1016/j.pmatsci.2022.101025
25. 25. Wood, D. L. (1997). CRC handbook of optical properties. CRC Press.